Spectrochimica Acta Part A: Molecular and Biomolecular Spectroscopy 329 (2025) 125581

Contents lists available at ScienceDirect

Spectrochimica Acta Part A:
Molecular and Biomolecular Spectroscopy

journal homepage: www.journals.elsevier.com/spectrochimica-acta-part-a-molecular-and-biomolecular-spectroscopy

Innovative method for provenance studies in cultural heritage: A new algorithm based on observables from high-resolution Raman spectra of red ochre

Francesca Assunta Pisu [a], Stefania Porcu [a,c,*], Raffaela Carboni [a], Valentina Mameli [b,c], Carla Cannas [b,c], Stefano Naitza [b], Rita Teresa Melis [b,d,e], Margherita Mussi [e,f], Daniele Chiriu [a]

[a] Department of Physics, University of Cagliari, 09042 Monserrato, Italy
[b] Department of Chemical and Geological Sciences, University of Cagliari, 09042 Monserrato, Italy
[c] National Interuniversity Consortium of Materials Science and Technology (INSTM), Cagliari Unit, 50121 Florence, Italy
[d] CNR-IGAG, Piazzale Aldo Moro 7, 00185 Rome, Italy
[e] Italo-Spanish Archaeological Mission at Melka Kunture and Balchit, Melka Kunture, Ethiopia
[f] ISMEO, Corso Vittorio Emanuele II 244, 00186 Rome, Italy

HIGHLIGHTS

- The non-destructive analysis of ochre-stained bones and non-flaked tools.
- The innovative application of high-resolution Raman spectroscopy.
- The development of a robust method for the provenance determination that leverages AI technology.

GRAPHICAL ABSTRACT

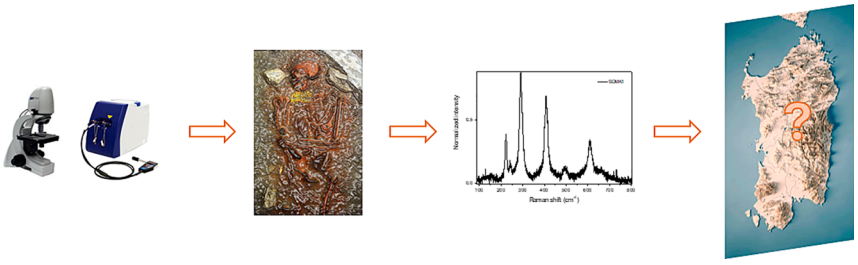

ARTICLE INFO

Keywords:
Ochre analysis
Non-destructive techniques
Provenance determination
Raman spectroscopy
Cultural heritage diagnostics
Artificial intelligence

ABSTRACT

Red ochre, typically derived from iron oxides and hematite, has been used since Pleistocene times for a range of different applications, practical as well as symbolic, including cave paintings and use in prehistoric burials. The importance to discover new methods for provenance determination, based on non-destructive portable techniques, represents a new challenge in the field of diagnostics of cultural heritage.

This study presents the data obtained from the analysis of several non-flaked tools and ochre-stained bones, showing evidence of ochre processing at the Mesolithic site of *S'omu e S'Orku* in Sardinia (Italy). To investigate the provenance of the ochre (hematite phase) found on a massive stone from the site and also used to cover the bones, we propose three distinct approaches derived from high-resolution Raman spectra of ochres, aiming to identify the maximum number of observables that can be reconducted to unicity criteria.

The reliability of this method enables the development of an automatic algorithm of Artificial Intelligence able to recognize the provenance of raw materials used in a range of activities. Furthermore, this study sheds light on one of the earliest and most distinctive Mesolithic burials uncovered in Sardinia to date, providing valuable insights into the human colonization of the island and the symbolic practices of its inhabitants during the Holocene epoch.

* Corresponding author at: Department of Physics, University of Cagliari, 09042 Monserrato, Italy.
E-mail address: stefania.porcu@dsf.unica.it (S. Porcu).

https://doi.org/10.1016/j.saa.2024.125581
Received 10 September 2024; Received in revised form 13 November 2024; Accepted 8 December 2024
Available online 10 December 2024

1. Introduction

In art analysis, whether examining contemporary pieces or those from antiquity like prehistoric artworks, procedures and pigment recipes serve as significant indicators of a specific period or artist. In studying compositional differences, the presence of additional compounds or elements can be clear evidence of the authorship of a particular work. The use of natural colours such as ochres [1,2], minerals and animal/plant dyes [3,4] can be a clue to mobility within a territory. When found in abundance, this suggests that they were easily available and possibly played a significant role in the activities of the time.

In such instances, identifying materials becomes more important due to the limited range of natural colors available. It necessitates a precise examination of the structural and compositional differences of these substances to ensure accurate attribution [5].

In the case of mineral pigments and rocks, it is possible to study the presence of major and minor (impurities) components and establish correlations between specific compositions and the geographical origins of the raw matter [6]. Additionally, variations in crystal structures can offer insights into the formation conditions of a particular geological source [7].

Analytical techniques such as microanalysis combined with scanning electron microscopy (SEM-EDX), X-ray diffraction (XRD), and infrared spectroscopy (FTIR-ATR) can be used for the quantitative or semi-quantitative study of the elements or compounds present in that material, which can detect compositional differences in minerals of different areas, if present [8–10]. Sometimes, no additive compounds or impurities can be detected from different sites, making the provenance identification difficult. It is then necessary to look at the structural differences related to the formation mechanism as a guide for the identification of the sourcing site. In addition to the previously mentioned methods, another promising technique is Raman spectroscopy [11,12]. By analyzing a Raman spectrum, various parameters such as intensity ratios, profile shapes, and peak positions can serve as distinguishing markers, highlighting differences among materials originating from different locations. A detailed study of this differences can be useful in developing a method for determining the provenance of materials.

In this work we propose a case study of the application of this new provenance approach based on the detailed study of the high-resolution Raman spectra [13]: the Mesolithic site of S'omu e S'Orku, in Sardinia (Italy), where some non-flaked tools and ochre-stained bones have been found, showing evidence of red ochre use [14].

Red ochre generally comes from iron oxides and, specifically, hematite powders and, in prehistoric times, has been used for a range of different applications, including cave paintings, symbolic use in burials, etc. [15]. From the excavation site the archaeologists extracted artifacts and bones exhibiting a distinct red coating layer that is not naturally associated with the local environmental rocks.

We selected three approaches to cluster the data: the first is the principal component analysis (PCA) clustering applied directly from the normalized Raman spectra, the second is based on the trend of the crystallinity of the hematite (intensity of the band at 220 cm^{-1}) *versus* purity ratio of hematite (ratio A_{660}/A_{610} between the areas of the bands at 600 and 610 cm^{-1}) and finally a more specific method based on the correspondence criteria of all the parameters chosen as markers for the identification such as position, area and full width at half maximum (FWHM).

For this method, we selected the observables from the Raman spectrum of hematite useful to identify the unicity criteria related to each sample. Once these distinctive criteria are identified, it is necessary to find the best assignation algorithm which can provide the required information about the provenance site of a particular mineral.

To support our provenance study, we used a multi-technique approach to analyze various rock samples as potential ochre sources. These samples were collected near the Mesolithic site of S'Omu e S'Orku (SOMK) and from several mineralized areas in western Sardinia. Our goal was to identify and distinguish the ochre sources used by the Mesolithic community under investigation.

2. Material and methods

2.1. Archaeological samples

The investigated ochre samples are from the *S'Omu e S'Orku* Mesolithic site (SOMK), a collapsed rock shelter in the Pleistocene aeolianite cliff on the southwestern coast of Sardinia (Fig. 1a) [14,16]. There are some hints to a possible human presence in the island during the late Pleistocene, but none is so far well dated. SOMK is one of the few early Holocene sites of Sardinia and the only one with a well dated substantial deposit, documenting the activities of prehistoric hunter-gatherer's groups. The stratigraphic sequence consists of debris slope and aeolian deposits with archaeological, faunal, and human remains including those of the heavily ochrated burial SOMK1 (Fig. 1b). Ochre use is consistent with the archaeological record of the time all over Europe, notably in funerary practices [17].

On top of jasper and obsidian lithic implements, an ochre crayon, ochre fragments, ochre-stained marine shells were also discovered, the latter ones as burial goods. The fauna is dominated by Prolagus sardus, an extinct endemic ochotonid the size of a hare. Because of the distance from the mainland, only a few endemic mammal species peopled Sardinia all over the Pleistocene and up to the early Holocene, before the arrival of Neolithic people who introduced new species.

Jasper and ochre outcrop in the San Pietro Island (about 50 km south) (Fig. 1a) which at the time was joined to the mainland [14,18].

- Three ochre samples (SOMK1, SOMK 22, 04CR) from SOMK were analysed: SOMK1 sample is from the skullcap of an adult-mature individual (SOMK1) whose skeleton is abundantly covered with ochre (Fig. 1b);
- 04CR sample is an ochre crayon (identifiable by shape) found near the SOMK1 human remains (Fig. 1c),
- SOMK22 is a small ochre aggregate from the uppermost part of the debris slope deposit the same level as SOMK 1 and close to it (Fig. 1d).

2.2. Reference samples

Eight iron oxide mineralized occurrences were sampled in different locations of western Sardinia to provide reference samples for our provenance study (Fig. 1a):

- Fe oxide ochraceous level from the Capo Becco deposit, San Pietro Island (*ochre CF*);
- hematite-bearing Jasper from the Capo Becco deposit, San Pietro Island (*Jasper CF*);
- ochraceous material in the Fe oxide zone of Monte Tamara sulfide deposit, Nuxis (*Nuxis MT*);
- Fe oxide-rich pisolithic paleosoil from Riu Bacchera mine, Nuxis (*Riu B.);*
- Fe oxide mineralization from hydrothermal vein in Capo Pecora, Arbus (*CP*);
- Fe oxide mineralization from Sant'Antonio hydrothermal vein in Montevecchio mine, Guspini (*MV*);
- Specularite from Montiferru (MF);
- Fe oxide-bearing metamorphic rocks of the SOMK basement (*schist*).

2.3. Raman and compositional analyses

High resolution micro-Raman scattering measurements were obtained in back scattering geometry through the confocal system SOL Confotec MR750 equipped with Nikon Eclipse Ni microscope. Raman

spectra were gathered by using, as excitation wavelength, the 785 nm line of an IO MatchBox series laser diode. The system is equipped with four gratings (150, 600, 1200 and 1800 grooves/mm) which can be selected depending on the measure requirements. The grating with 1800 grooves/mm was used to obtain a resolution of 0.2 cm^{-1}.

For each experimental setup, all the spectra were collected with an acquisition time of about 60 s (five replicas) and the final spectra obtained as the average of the five 60 s-long scans. The power excitation was between 5 and 10 mW concentrated in a spot of 0.3 mm^2 on the surface through a Raman Video Micro-Sampling System (Nikon Eclipse for high-resolution and BAC151B in the other case) equipped with a 20 × Olympus objective to select the area on the samples. Each measurement area represents a sampling surface of about 1 cm^2.

2.4. SEM-EDS measurements

SEM-EDS were gathered by a scanning electron microscope ESEM: FEI Quanta 200 under low vacuum conditions. EDS semiquantitative analyses were obtained with the help of Thermo Scientific EDS UltraDry INTX-10P-A system equipped with Pathfinder. Each point of analysis was collected with an acceleration voltage of 20 kV and live time of 30 s.

2.5. Powder X-ray diffraction (PXRD)

Powder X-ray Diffraction (PXRD) analyses were carried out by using a PANalytical X'pert Pro (Malvern PANalytical, Malvern, UK) equipped with Cu Kα radiation (1.5418 Å). The qualitative analysis of the PXRD patterns was performed by comparison of the experimental data and the PDF database from ICSD by using the Xpert High Score software.

2.6. Attenuated total reflectance (ATR)

Infrared spectra were obtained by Attenuated Total Reflectance (ATR) Agilent Cary 630 spectrophotometer equipped with an ATR module in the range 650–4000 cm^{-1}. The spectra were processed with Microlab PC (v 5.5.1989, Agilent, Santa Clara, CA, USA).

2.7. Deconvolutions and PCA clustering

Lorentzian deconvolutions were made by means of the OriginLAB

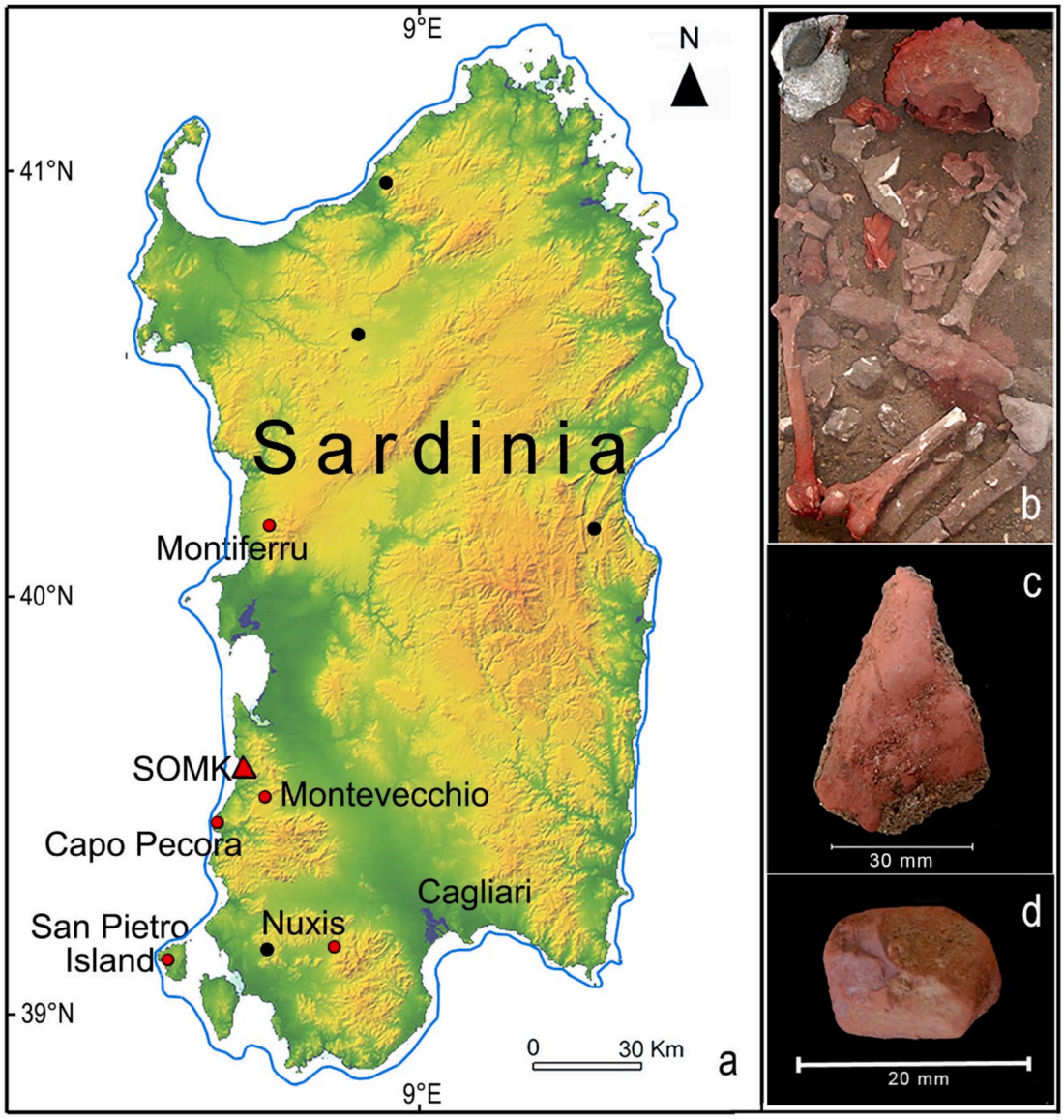

Fig. 1. (a) Location map of the *S'Omu e S'Orku* (SOMK) site and the outcrops of the rock samples analysed, blue color line represents the palaeocoastline of Mesolithic period at −20 m: (b) human remains covered with ochre (SOMK1); c) ochre crayon sample (04CR); d) ochre aggregate sample (SOMK22).

2021 software through the Levemberg Marquardt iteration algorithm with 500 iterations and 10^{-9} as tolerance. PCA analysis was made also with the help of OriginLAB 2021 software with simple descriptive statistics and the use of correlation matrix. Before the PCA analysis the data were normalized to the most intense peak (292 cm^{-1}).

3. Results and discussion

XRD pattern of *SOMK1* in comparison with those of the geological sources and the results of the qualitative analysis are reported in Fig. 2 (left side) and Table 1, respectively. *SOMK1* exhibit the presence of hematite (α-Fe_2O_3, PDF card # 00-033-0664) together with quartz (SiO_2, PDF card # 00-033-1161), calcite ($CaCO_3$, PDF card # 00-005-0586), ordered albite ($NaAlSi_3O_8$, PDF card # 00-009-0466), muscovite-*3T* ($(K,Na)(Al,Mg,Fe)_2(Si_{3.1}Al_{0.9})O_{10}(OH)_2$, PDF card # 00-007-0042), and kaolinite-*1A* ($Al_2Si_2O_5(OH)_4$, PDF card # 00-014-0164). Other possible additional phases might be present, such as microcline, but the low intensity of the diffraction peaks and the complex matrix with possible overlapping of the patterns of different crystalline phases hamper a certain assignment of the minor components. Hematite is also present in all geological samples but *MV*, that instead does contain mainly goethite (and quartz), and *schist*, which features only quartz and silicoaluminates (albite, muscovite, kaolinite). The absence of XRD peaks ascribable to hematite in these latter samples suggests a content below the limit of detection, presumably below 5 %w/w. Besides the ubiquitous presence of quartz, the geological samples have different mineralogical composition with the purest hematite found for *ochre CF* (*i.e.*, only quartz as secondary phase), which exhibits also quite broad peak, suggesting the presence of hematite in form of nanocrystallites. Concerning the additional crystalline phases found in SOMK1, no perfect matching is observed with the mineralogical composition of the geological sources. In particular, calcite was found in the Nuxis Riu B.; ordered albite is present in schist; both Nuxis MT and schist show the presence of muscovite, whereas kaolinite was detected in Nuxis samples,

Table 1
Qualitative analysis of the XRD patterns of SOMK1 and the geological samples. H: hematite (α-Fe2O3, PDF card # 00-033-0664); Q: quartz (SiO2, PDF card # 00-033-1161); C: calcite (CaCO3, PDF card # 00-005-0586); A: ordered albite (NaAlSi3O8, PDF card # 00-009-0466); M: muscovite-3T ((K,Na)(Al,Mg,Fe)2(Si3.1Al0.9)O10(OH)2, PDF card # 00-007-0042); G: goethite (α-FeOOH, PDF card # 00-029-0713); B: barite (BaSO4, PDF card # 00-005-0448); K: kaolinite-1A (Al2Si2O5(OH)4, PDF card # 00-014-0164).

Sample\Mineral	H	Q	C	A	M	G	B	K
SOMK1	x	x	x	x	x	–	–	x
Ochre CF	x	x	–	–	–	–	–	–
MV	–	x	–	–	–	x	–	–
Nuxis MT	x	x	–	–	x	x	–	x
CP	x	x	–	–	–	x	–	–
Nuxis Riu B.	x	x	x	–	–	–	x	x
Jasper CF	x	x	–	–	–	x	x	–
MF	x	x	–	–	–	–	–	x
Schist	–	x	–	x	x	–	–	x

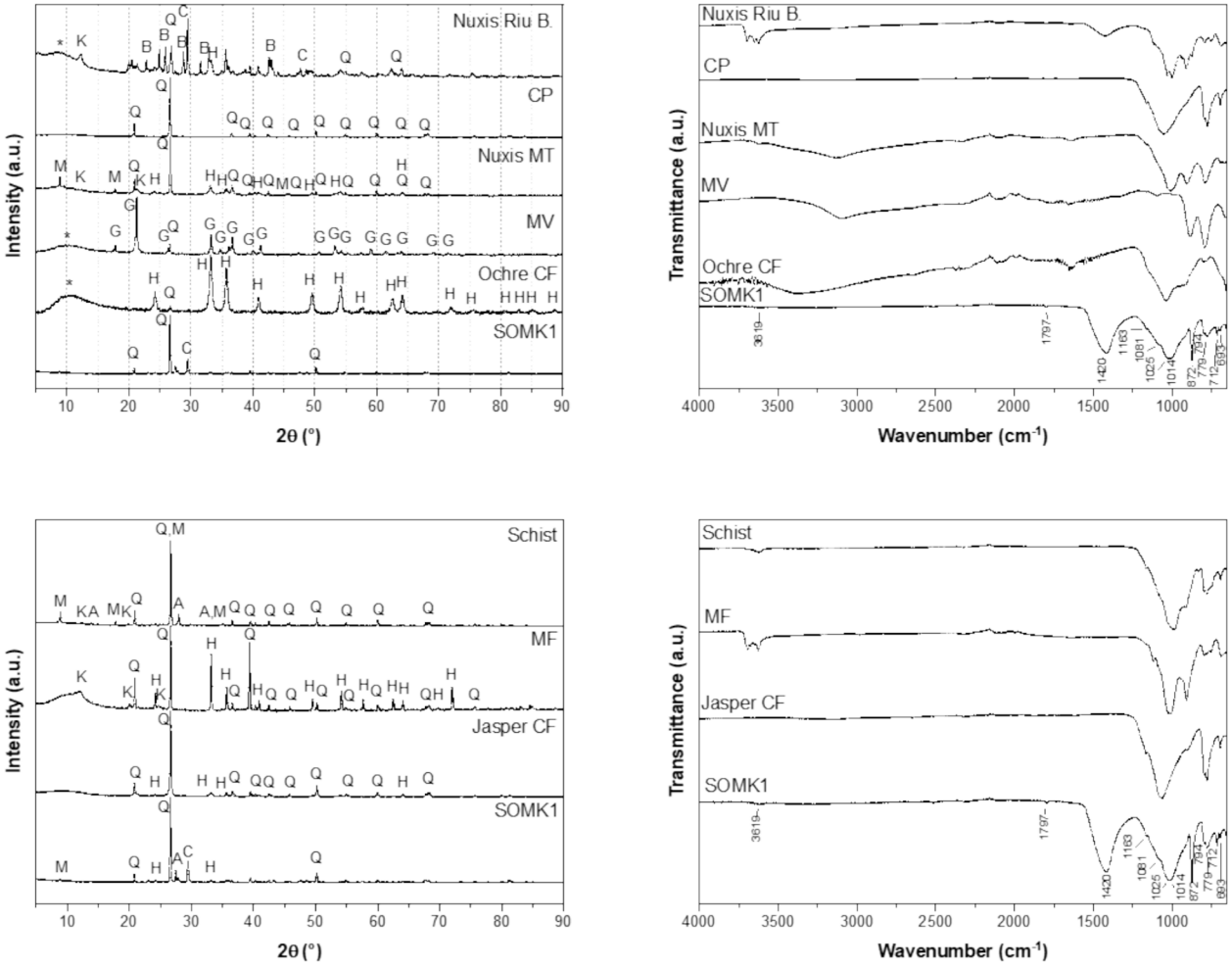

Fig. 2. XRD patterns (left) and ATR spectra (right) of SOMK1 and the geological samples used as reference samples for our provenance study. The symbol (*) in the XRD patterns identifies the contribution of the plexiglass sample holder.

MF, and schist. It is worthy to note that the presence of these additional crystalline phases in SOMK1 might arise from a soil contamination (sandy concretion with quartz grains, feldspars, lithic fragments of basement metamorphic rocks, and fragments of Prolagus). Goethite, barite, and dolomite, detected in some of the geological sources, were not detected in SOMK1.

To further confirm the mineralogical composition of the samples by another independent technique, ATR analyses were carried out and the collected spectra are reported in Fig. 2(right side). The spectrum of SOMK1 shows bands at 3619 cm^{-1}, 1797 cm^{-1}, 1420 cm^{-1}, 1163 cm^{-1} (shoulder), 1081 cm^{-1}, 1025 cm^{-1}, 1014 cm^{-1}, 872 cm^{-1}, 794 cm^{-1}, 779 cm^{-1}, 712 cm^{-1}, and 693 cm^{-1}, which can be ascribed to the presence of calcite, quartz, and kaolinite, in agreement with the XRD results. The absence of bands associated with albite and muscovite can be explained by the overlapping of the vibrational modes of the aluminosilicates, as reported in Table S1. The highest noise in the spectra was obtained for the Ochre CF sample, with the evidence of the water molecules vibrational mode, probably due to the higher hematite content, whose bands are not visible in the investigated range (4000–650 cm^{-1}). In addition, the predominance of goethite in the MV sample was also confirmed, with an almost complete overlapping of the spectrum with that of a synthesised goethite sample, used as a reference (Fig. S1) together with the presence of quartz (vibrational mode at 1092 cm^{-1}). On the basis of the XRD and ATR analysis it was not possible to evidence similarities between the archaeological sample and the geological ones, since these techniques are affected by the presence of crystalline phases other than iron oxides and are able mainly to characterize the matrixes of the samples. Therefore, Raman spectroscopy was chosen as characterization method able to focus on the hematite phase, responsible for the coloured artifacts.

Raman spectroscopy was applied directly on the archaeological samples without the need of a sampling procedure, differently to what done with XRD and FTIR-ATR analyses conducted on the powder sample SOMK1. This approach allowed the analysis of SOMK22 and the red crayon 04CR in addition to SOMK1.

Experimental results from Raman measurements are reported in Fig. 3 where their Raman spectra are characterized by seven peaks at around 221, 239, 290, 401, 487, 604, and 661 cm^{-1} easily assigned to the characteristic spectrum of Fe_2O_3 in the hematite phase as reported by numerous works in the literature [19–21]. These findings have been further confirmed by EDS and XRF analysis which shows the presence of both iron and oxygen elements. All frequencies composing the spectrum, and relative assignation of the vibrational modes are summarized in Table 2.

A detailed analysis confirms the presence of two classes of Raman active modes of hematite in the region 200–700 cm^{-1}. In particular, the characteristic bands at 221 and 491 cm^{-1} are attributed to A1g modes, while bands at 239, 287, 401, and 605 cm^{-1} to Eg vibrations. Low-frequency modes (200–300 cm^{-1}) are assigned to Fe atom vibrations, while bands in 400–650 cm^{-1} are assigned to O atom vibrations. As reported in the literature, $A1_g$ band at 221 cm^{-1} is ascribed to the movement of iron cations along c-axis. E_g bands at 401 cm^{-1} and 605 cm^{-1} are assigned to symmetric mode of O atoms relative to other cations in a plane perpendicular to crystallographic c-axis and Fe-O stretching vibrations, respectively.[22].

The shifting of bands position is a function of grains dimensions which causes the variation in frequency due to phonon confinement. All the three samples show the same characteristic spectrum for the red hematite except the crayon (04CR-sample) that presents a further intense band at around 353 cm^{-1} due to additive compounds compatible with a mixture of sulphides such as arsenopyrite [23,24].

To conduct a provenance study of the hematite phase ochre found on the mentioned three archaeological samples, the burial (SOMK1), crayon (04CR) and a red pebble found close to the SOMK1 level, we propose three different approaches with a comparative discussion about the results. The approaches are based on correspondence criteria, PCA clustering and the curve crystallinity *versus* purity ratio of hematite. In our study, we considered eight different iron oxide mineralization samples from various locations in western Sardinia as reference points. These reference samples, denoted as ochre CF, Jasper CF, Nuxis MT, Riu B., CP, MV, MF, and schist, were analyzed to identify potential sources of ochre for the SOMK sample.

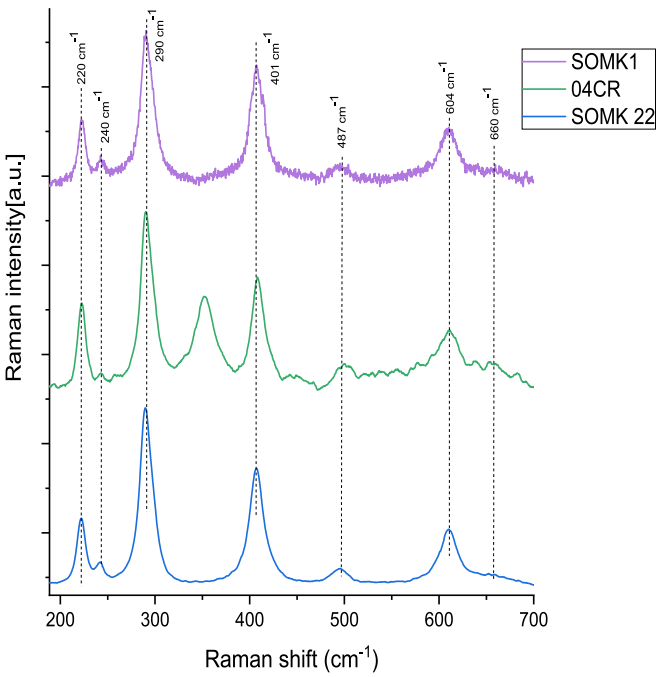

Fig. 3. High resolution Raman spectra of the archaeological samples obtained with a 785 nm excitation laser. In blue the Raman spectrum of SOMK22 sample, in green the Raman spectrum of 04CR sample and in purple the Raman spectrum of SOMK1 sample.

Table 2
Raman modes of hematite.

Frequencies (cm^{-1})	Vibrational mode assignation
221.0	A1g
239.3	Eg
287.2	Eg
401.6	Eg
487.6	A1g
604.1	Eg
661.4	1LO Eu

3.1. Principal component analysis (PCA)

The first method proposed is based on a multivariate analysis through PCA of the Raman spectra obtained with high resolution for all the samples [25,26]. In this way, we can obtain a clustering of our samples which pools them for their affinity on two principal components (Fig. 4). This PCA reveals a possible clustering only if we observe the Principal component 2, without obtaining any precise assignation. It is clearly discernible the presence of four different groups in Fig. 3, in particular the samples from SOMK (SOMK22, SOMK1, 04CR) are closer to the jasper of San Pietro Island, giving a first indication of the provenance of the employed ochre and also a hint about the clustering of the three different archaeological items. The PCA result is only a first indicative attempt of clusterization that could be affected by artefacts on the extraction of data.

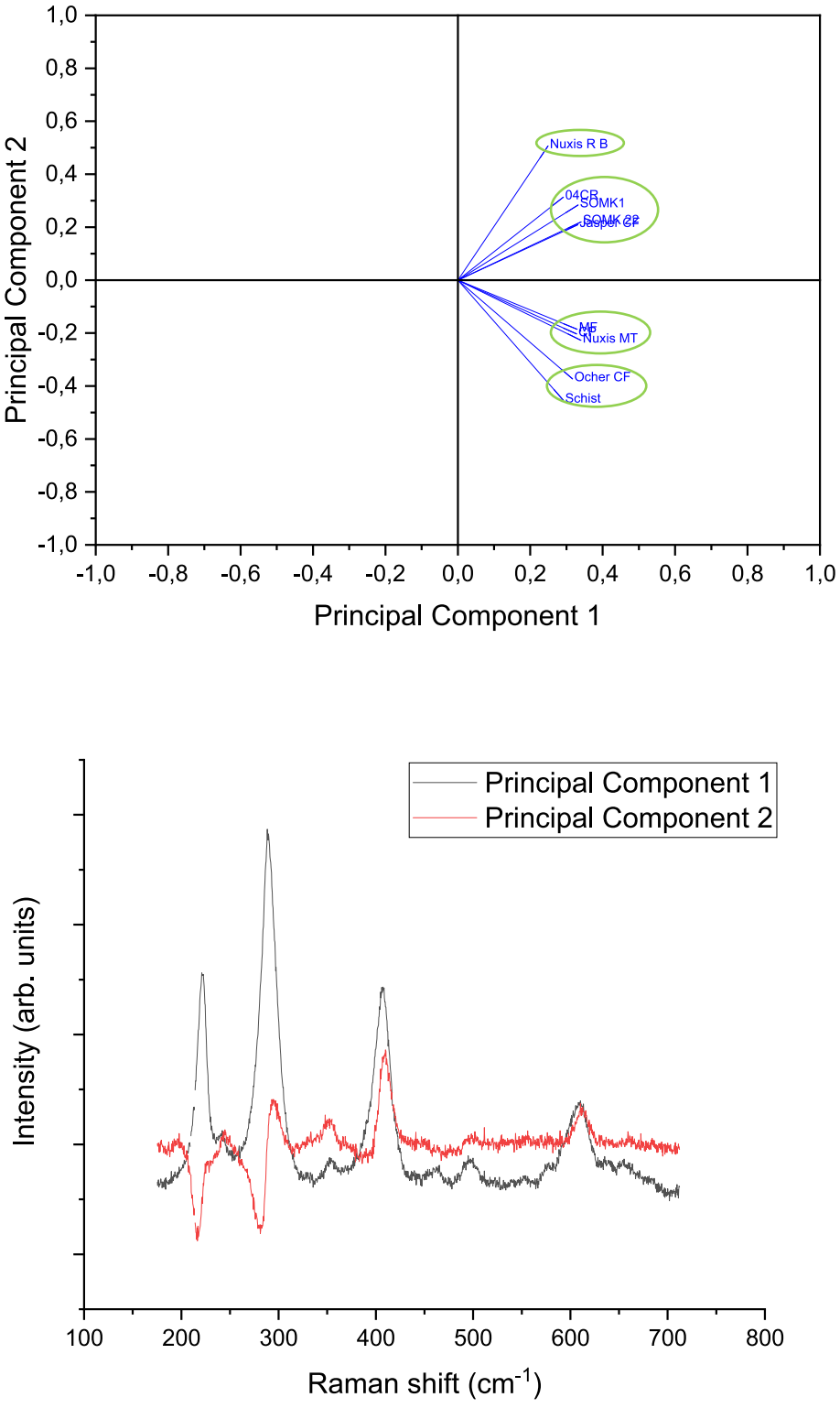

Fig. 4. PCA analysis resulting from the analysis of Principal Components 1 and 2.

3.2. *Crystallinity versus purity ratio of hematite*

The second method is based on the plot of the FWHM of the band at 220 cm^{-1} taken from the Raman spectra of each sample with respect to the purity ratio between areas A_{610}/A_{660} which represents the purity grade of hematite crystal. Fig. 5 shows the points determined for all the samples.

From the graph, we can distinguish a good crystallinity of our archaeological samples, which corresponds to a low value of FWHM for the band at 220 cm^{-1} and an impurity grade of less than 30 %. The lowest crystallinity is attributed to Nuxis Riu B ochre while the highest value of impurity grade is associated with Nuxis Monte Tamara and local schist. The experimental points evidence how the average purity is about 20–30 % for our ancient samples. In addition, for what concerns our relics, the crystallinity and the purity grade are close to those obtained for Montiferru, Jasper, and Ochre from San Pietro Island. Actually,

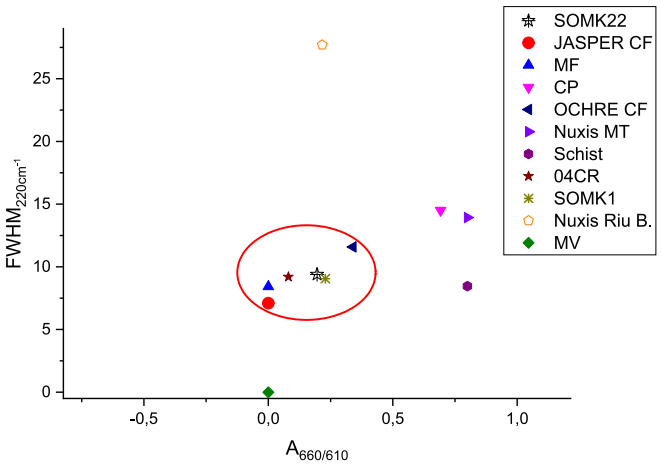

Fig. 5. Crystallinity *versus* purity ratio clustering: points are obtained by plotting the FWHM at 220 cm^{-1} in relation to the ratio between the band areas A_{660} and A_{610} of the Raman spectra.

through a simple clustering operation based on the distance among the experimental points, we can pool them to these sites, but without providing a possible and definitive assignation.

3.3. Correspondence criteria

The last method starts from the high-resolution Raman spectra and by identifying the maximum number of observables that can be reconducted to unicity criteria. Starting from the normalized Raman spectrum of reference (SOMK1) we performed a deconvolution of the experimental data employing Lorentzian profiles which analytic expression is done in Eq. (1):

$$y = y_0 + \frac{2A}{\pi}\frac{w}{4(x-x_c)^2 + w^2} \quad (1)$$

where parameters A, x_c, and w represent the area, peak centre, and width respectively (Fig. 6a).

After deconvolution operations, we identified all the position x_c of found 7 peaks with relative FWHM, and we calculated the area ratios concerning the normalization peak with the highest intensity (peak 3). At the end of this process, we obtained 20 parameters (7 peak positions, 6 area ratios, and 7 FWHM) that can be used as criteria to assign the correspondence. We imposed conditional limits to the parameters and associate a score for each section (peak, area ratios, and FWHM) if the condition is respected. The condition can be varied to restrict the field of score assignation and refine the result. Fig. 6b shows the algorithm of score assignation, where we used as limits for the peak positions four different conditions:

$$\Delta x_c < 0.5,\ 1,\ 2,\ 3\ cm^{-1};\ \frac{\Delta R}{R} < 30\%\ \text{with}\ R = \frac{A_i}{A_3},\ \text{and}\ \frac{\Delta FWHM}{FWHM} < 30\%.$$

We also decide to enhance the method considering the peak position as a predominant criterion of matching: the area ratios and FWHM values are evaluated only for those peaks that respect the first grade of confidence in the position. Lastly, to refine the method, we can introduce also a weighted score which allows to change the desired weight of each criterion, thus the final weighted score matching (WSM) can be expressed as follow:

$$WSM = \frac{w_{peak}S_{peak} + w_R S_R + w_{FWHM}S_{FWHM}}{w_{peak}(totalnr.peaks) + w_R(totalnr.R) + w_{FWHM}(totalnr.FWHM)}$$

Table S2 represents a synoptic comparison of all criteria found for each sample in which we operated the assignation, and we determined a weighted score on the basis of the effective correspondence. The range of confidence for the assignment is$\Delta x_c < 3\ cm^{-1}$, and a relative variation for area ratio and FWHM ratio < 30 %. These values are chosen to take into account the deconvolution error standard and the spectrograph resolution. The matching reported in the table was calculated as the percentage ratio between the total weighted score determined for each sample and the total number of weighted defined criteria. From this table it is evident that two cases are the most probable assignations concerning the other samples: Jasper CF and Montiferru. The method allows to refine the results by using more stringent conditions (see Fig. 7).

By reducing only the confidence of the first criterion associated with the peak position, we can discriminate the best matching. The graphs show the value of the total matching of the samples varying only in the position confidence from 3 to 0.5 cm^{-1}. As evidenced in the histograms the highest value of matching corresponds to Jasper CF which presents always the highest percentage of each case. Moving at the lowest confidence range of 0.5 cm^{-1}, we observe a degeneration out of the trend only for SOMK22, which we attributed to an excessive restriction of this criterium. However, for confidence below 1 cm^{-1}, Jasper CF is again the

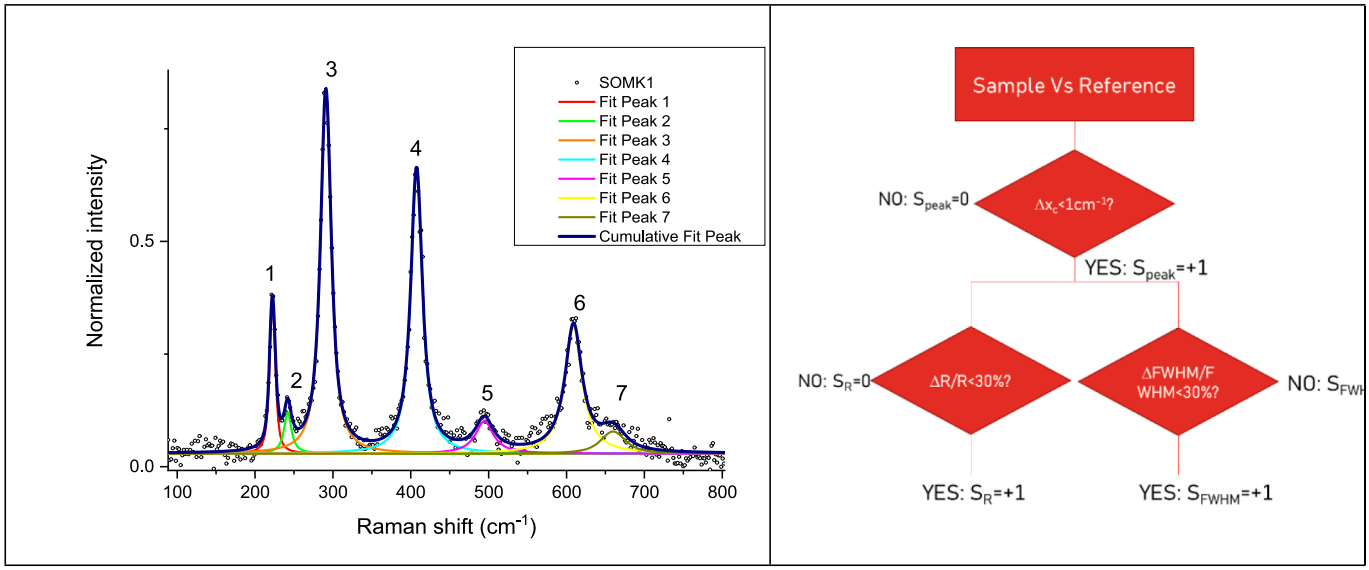

Fig. 6. (a) Deconvolution of Raman spectrum by Lorentzian profiles; (b) algorithm of score assignation for the correspondence criteria method.

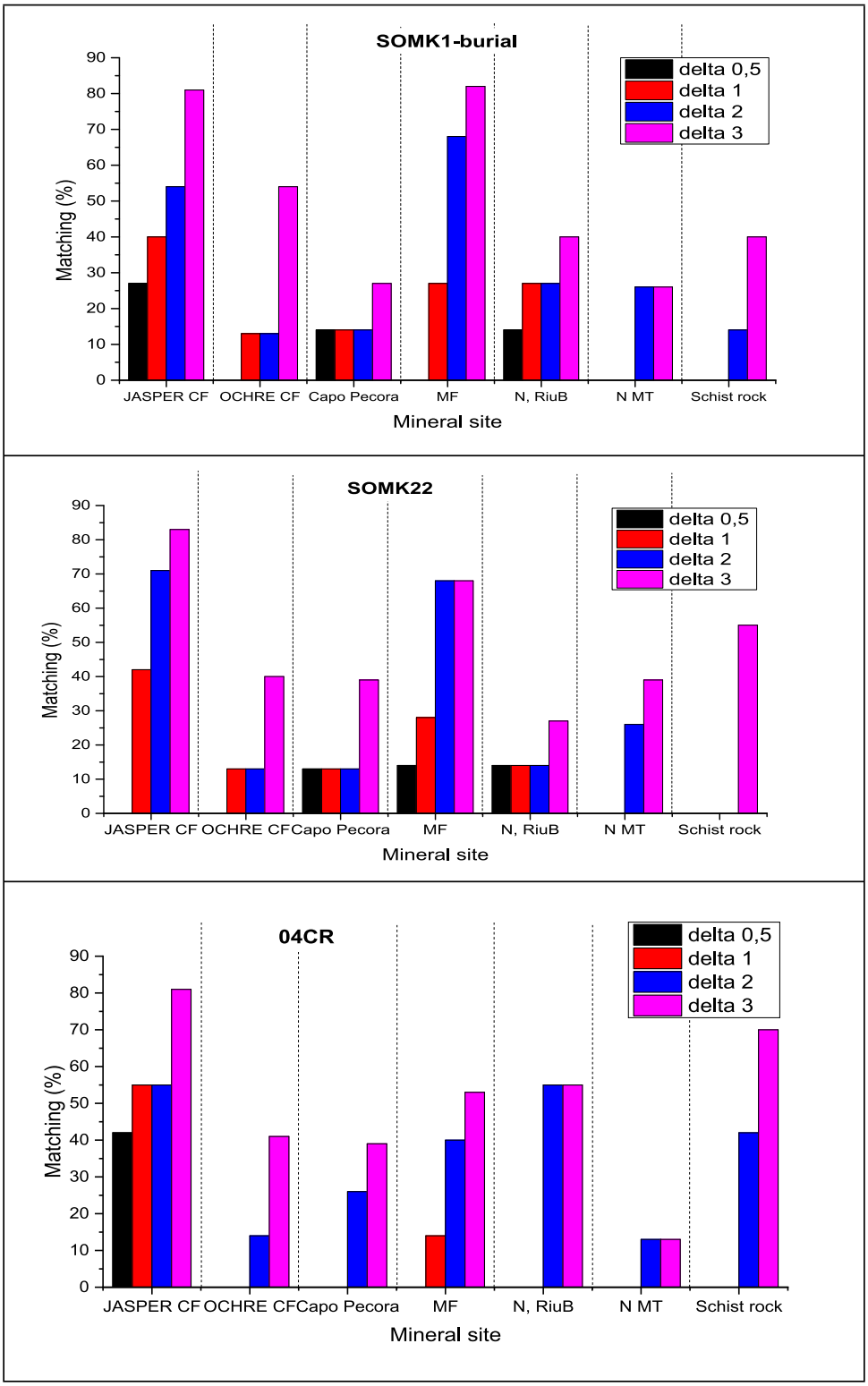

Fig. 7. Histograms of matching as a function of x_c-confidence values.

higher matching site, as the other samples confirmed.

This result is further corroborated by the EDS and XRF analyses detailed in the Supporting information (Tables S3 and S4), particularly in terms of the ratio between iron and silicon elements present in the samples. This parameter indicates the percentage content of iron oxides relative to the total silicate component. As shown in the Tables S3 and S4, SOMK1 and 04CR closely resemble Jasper CF. However, the uncertainty associated with SOMK22 is confirmed, suggesting potential contamination by elements from Ochre CF or MV, the only sites exhibiting a higher Fe/Si ratio.

4. Conclusions

The three proposed methods, derived from the high-resolution

Raman spectra, demonstrated varying degrees of reliability in attributing archaeological samples. Principal Component Analysis (PCA) emerged as the most generic and least suitable method for this small sample size, primarily because it only suggested a non-specific clustering without providing detailed insights into the provenance of the samples. This limitation highlights the challenge of using PCA for definitive conclusions in studies with limited datasets.

On the other hand, the crystallinity method offered a more nuanced differentiation of sample variability. By assessing the degree of crystallinity, this method was able to indicate a set of proximities derived from the purity levels of the samples. This approach revealed similarities between the archaeological samples and those from the CF (Cave Formation) and MF (Mineral Formation) sites, suggesting that the purity of the samples could serve as a distinguishing factor for provenance studies.

The most promising results were obtained from the third method, which involved weighted matching criteria based on the profile differences in the Raman spectra. This approach provided a more definitive attribution of provenance by closely analyzing the spectral profiles. By weighting the differences in the Raman spectra, this method could accurately match the archaeological samples to their potential sources, offering a high level of specificity and reliability.

In summary, while PCA offered a broad, non-specific clustering that proved less useful for a small number of samples, the crystallinity method and the weighted matching criteria demonstrated greater potential for accurately attributing archaeological samples. The crystallinity method highlighted the importance of sample purity in distinguishing provenance, whereas the weighted matching criteria method delivered a precise and definitive attribution based on detailed spectral analysis.

While our analysis suggests that the weighted matching method shows promise for provenance attribution, we acknowledge that the limited sample size necessitates caution in our conclusions, and further studies with a larger dataset are essential to validate its effectiveness as a preferred method. Additionally, we highlight the value of complementary approaches, such as the crystallinity method, to enhance our understanding of sample variability.

These findings underscore the value of employing multiple complementary methods to achieve reliable results in the study of archaeological sample provenance.

CRediT authorship contribution statement

Francesca Assunta Pisu: Data curation, Formal analysis, Investigation, Methodology, Writing – original draft. **Stefania Porcu:** Conceptualization, Investigation, Writing – original draft, Validation, Visualization, Writing – review & editing. **Raffaela Carboni:** Data curation, Formal analysis. **Valentina Mameli:** Data curation, Formal analysis, Writing – review & editing. **Carla Cannas:** Data curation, Formal analysis, Writing – review & editing. **Stefano Naitza:** Investigation, Validation, Visualization, Writing – review & editing. **Rita Teresa Melis:** Investigation, Validation, Visualization, Writing – review & editing. **Margherita Mussi:** Investigation, Validation, Visualization, Writing – review & editing. **Daniele Chiriu:** Conceptualization, Investigation, Methodology, Supervision, Validation, Visualization, Writing – original draft, Writing – review & editing.

Declaration of competing interest

The authors declare that they have no known competing financial interests or personal relationships that could have appeared to influence the work reported in this paper.

Acknowledgements

We are grateful to Gruppo Archeologico Neapolis (Guspini) for the continuous support. The research permits were awarded through Soprintendenza Archeologia Belle arti e Paesaggio per la città metropolitana di Cagliari e per le province di Oristano e Sud Sardegna (ConcessioneProt. N° 591 del 18.05.2022 del Ministero Beni culturali).

Appendix A. Supplementary material

Supplementary data to this article can be found online at https://doi.org/10.1016/j.saa.2024.125581.

Data availability

Data will be made available on request.

References

[1] D.E. Rosso, A.P. Martí, F. D'Errico, Middle stone age ochre processing and behavioural complexity in the horn of Africa: evidence from porc-epic cave, dire dawa, Ethiopia, PLoS One 11 (2016) 1–35, https://doi.org/10.1371/journal.pone.0164793.
[2] S. Wolf, R. Dapschauskas, E. Velliky, H. Floss, A.W. Kandel, N.J. Conard, The use of ochre and painting during the upper paleolithic of the Swabian Jura in the context of the development of ochre use in Africa and Europe, Open Archaeol. 4 (2018) 185–205, https://doi.org/10.1515/opar-2018-0012.
[3] J.M. Grünberg, Middle Palaeolithic birch-bark pitch, Antiquity (2002), https://doi.org/10.1017/s0003598x00089638.
[4] D. Urem-Kotsou, S. Mitkidou, E. Dimitrakoudi, N. Kokkinos, M. Ntinou, Following their tears: production and use of plant exudates in the Neolithic of North Aegean and the Balkans, Quat. Int. (2018), https://doi.org/10.1016/j.quaint.2018.10.027.
[5] L. Nannan, W. Qirou, Z. Jingna, L. Shuqin, L. Junyu, C. Haixia, Insight into the progress on natural dyes: sources, structural features, health effects, challenges, and potential, Molecules 27 (2022).
[6] N. Etemad-Saeed, M. Hosseini-Barzi, J.S. Armstrong-Altrin, Petrography and geochemistry of clastic sedimentary rocks as evidences for provenance of the Lower Cambrian Lalun Formation, Posht-e-badam block, Central Iran, J. Afr. Earth Sci. (2011), https://doi.org/10.1016/j.jafrearsci.2011.06.003.
[7] A. Needham, S. Croft, R. Kröger, H.K. Robson, C.C.A. Rowley, B. Taylor, A. Gray, C. Conneller, The application of micro-Raman for the analysis of ochre artefacts from Mesolithic palaeo-lake Flixton, J. Archaeol. Sci. Rep. 17 (2018) 650–656, https://doi.org/10.1016/j.jasrep.2017.12.002.
[8] A. Ali, Y.W. Chiang, R.M. Santos, X-ray diffraction techniques for mineral characterization: a review for engineers of the fundamentals, applications, and research directions, Minerals 12 (2022), https://doi.org/10.3390/min12020205.
[9] A. Ali, N. Zhang, R.M. Santos, Mineral characterization using scanning electron microscopy (SEM): a review of the fundamentals, advancements, and research directions, Appl. Sci. 13 (2023), https://doi.org/10.3390/app132312600.
[10] T. Note, Geochemistry, Technical Note FTIR for Mineral Identification, 2022.
[11] N.K. Lünsdorf, J. Kalies, P. Ahlers, I. Dunkl, H. von Eynatten, Semi-automated heavy-mineral analysis by Raman spectroscopy, Minerals (2019), https://doi.org/10.3390/min9070385.
[12] C. Carey, T. Boucher, S. Mahadevan, P. Bartholomew, M.D. Dyar, Machine learning tools formineral recognition and classification from Raman spectroscopy, J. Raman Spectrosc. (2015), https://doi.org/10.1002/jrs.4757.
[13] S. Andò, E. Garzanti, Raman spectroscopy in heavy-mineral studies, Geol. Soc. Spec. Publ. 386 (2014) 395–412, https://doi.org/10.1144/SP386.2.
[14] MESOLITICOARBUSHalle.pdf, n.d.
[15] A. Needham, S. Croft, R. Kröger, H.K. Robson, C.C.A. Rowley, B. Taylor, A. G. Jones, C. Conneller, The application of micro-Raman for the analysis of ochre artefacts from Mesolithic palaeo-lake Flixton, J. Archaeol. Sci. Rep. 17 (2018) 650–656, https://doi.org/10.1016/j.jasrep.2017.12.002.
[16] R.T. Melis, V. Demurtas, M. Mussi, P. Emanuele Orrù, A. Sulis, F. Altamura, R. Erbì, M. Orrù, G. Deiana, The paleolandscape evolution of the southwestern coast of Sardinia (Italy) and its impact on Mesolithic settlements, J. Maps 19 (2023) 1–14, https://doi.org/10.1080/17445647.2023.2182722.
[17] M. Bestattungen, Mesolithic burials – Rites, symbols and social organisation of early postglacial communities Mesolithische Bestattungen – Riten , Symbole und soziale, 2013.
[18] G. Deiana, L. Lecca, R.T. Melis, M. Soldati, V. Demurtas, P.E. Orrù, Submarine geomorphology of the southwestern Sardinian continental shelf (Mediterranean sea): insights into the last glacial maximum sea-level changes and related environments, Water (Switzerland) 13 (2021), https://doi.org/10.3390/w13020155.
[19] I. Chamritski, G. Burns, Infrared- and Raman-active phonons of magnetite, maghemite, and hematite: a computer simulation and spectroscopic study, J. Phys. Chem. B (2005), https://doi.org/10.1021/jp048748h.
[20] A.M. Jubb, H.C. Allen, Vibrational spectroscopic characterization of hematite, maghemite, and magnetite thin films produced by vapor deposition, ACS Appl. Mater. Interfaces (2010), https://doi.org/10.1021/am1004943.
[21] C.P. Marshall, W.J.B. Dufresne, C.J. Rufledt, Polarized Raman spectra of hematite and assignment of external modes, J. Raman Spectrosc. (2020), https://doi.org/10.1002/jrs.5824.

[22] I.V. Chernyshova, M.F. Hochella, A.S. Madden, Size-dependent structural transformations of hematite nanoparticles. 1. Phase transition, PCCP 9 (2007) 1736–1750, https://doi.org/10.1039/b618790k.
[23] M. Moroni, S. Naitza, G. Ruggieri, A. Aquino, P. Costagliola, G. De Giudici, S. Caruso, E. Ferrari, M.L. Fiorentini, P. Lattanzi, The Pb-Zn-Ag vein system at Montevecchio-Ingurtosu, southwestern Sardinia, Italy: a summary of previous knowledge and new mineralogical, fluid inclusion, and isotopic data, Ore Geol. Rev. 115 (2019) 103194, https://doi.org/10.1016/j.oregeorev.2019.103194.
[24] M.L. Deidda, S. Naitza, M. Moroni, G.B. De Giudici, D. Fancello, A. Idini, A. Risplendente, Mineralogy of the scheelite-bearing ores of Monte Tamara, SW Sardinia: insights for the evolution of a Late Variscan W–Sn skarn system, Mineral. Mag. 87 (2023) 86–108, https://doi.org/10.1180/mgm.2022.119.
[25] A. Coccato, M.C. Caggiani, An overview of Principal Components Analysis approaches in Raman studies of cultural heritage materials, J. Raman Spectrosc. 55 (2024) 125–147, https://doi.org/10.1002/jrs.6621.
[26] J. Riu, B. Giussani, Analytical chemistry meets art: the transformative role of chemometrics in cultural heritage preservation, Chemom. Intell. Lab. Syst. 247 (2024) 105095, https://doi.org/10.1016/j.chemolab.2024.105095.